JGR Atmospheres

RESEARCH ARTICLE
10.1029/2024JD041260

Intermediate Fluence Downward Terrestrial Gamma Ray Flashes as Observed by the Telescope Array Surface Detector

R. U. Abbasi[1], N. Kieu[1], P. R. Krehbiel[2], J.W. Belz[3], M. M. F. Saba[4], W. Rison[2], M. A. Stanley[2], D. Rodeheffer[2], D. Mazzucco[1], T. Knight[1], D. R. da Silva[4], I. T. Cruz[4], J. Remington[3,5], J. Mazich[1], R. LeVon[3], K. Smout[3], A. Petrizze[3], E. Mattos[6], T. Abu-Zayyad[1,3], M. Allen[3], R. Arimura[7], E. Barcikowski[3], D. R. Bergman[3], S. A. Blake[3], I. Buckland[3], B. G. Cheon[8], M. Chikawa[9], T. Fujii[7,10], K. Fujisue[9], K. Fujita[9], R. Fujiwara[7], M. Fukushima[9], G. Furlich[3], N. Globus[11,12], R. Gonzalez[3], W. Hanlon[3], N. Hayashida[13], H. He[11], K. Hibino[13], R. Higuchi[11], K. Honda[14], D. Ikeda[13], N. Inoue[15], T. Ishii[14], H. Ito[11], D. Ivanov[3], H. Iwakura[16], A. Iwasaki[7], H. M. Jeong[17], S. Jeong[17], C. C. H. Jui[3], K. Kadota[18], F. Kakimoto[13], O. Kalashev[19], K. Kasahara[20], S. Kasami[21], S. Kawakami[7], K. Kawata[9], I. Kharuk[19], E. Kido[11], H. B. Kim[8], J. H. Kim[3,22], J. H. Kim[3], S. W. Kim[17], Y. Kimura[7], I. Komae[7], Y. Kubota[16], M. Kuznetsov[19,23], Y. J. Kwon[24], K. H. Lee[17], B. Lubsandorzhiev[19], J. P. Lundquist[3,25], T. Matsuyama[7], J. N. Matthews[3], R. Mayta[7], I. Myers[3], S. Nagataki[11], K. Nakai[7], R. Nakamura[16], T. Nakamura[26], A. Nakazawa[16], E. Nishio[21], T. Nonaka[9], S. Ogio[9], M. Ohnishi[9], H. Ohoka[9], Y. Oku[21], T. Okuda[27], Y. Omura[7], M. Ono[11], A. Oshima[28], S. Ozawa[29], I. H. Park[17], M. Potts[3,30], M. S. Pshirkov[19,31], D. C. Rodriguez[3], C. Rott[3,17], G. I. Rubtsov[19], D. Ryu[32], H. Sagawa[9], N. Sakaki[9], T. Sako[9], N. Sakurai[7], T. Seki[16], K. Sekino[9], P. D. Shah[3], Y. Shibasaki[16], N. Shibata[21], T. Shibata[9], J. Shikita[7], H. Shimodaira[9], B. K. Shin[32], H. S. Shin[9], D. Shinto[21], J. D. Smith[3], P. Sokolsky[3], B. T. Stokes[3], T. A. Stroman[3], K. Takahashi[9], M. Takamura[33], M. Takeda[9], R. Takeishi[9], A. Taketa[34], M. Takita[9], Y. Tameda[21], K. Tanaka[35], M. Tanaka[36], S. B. Thomas[3], G. B. Thomson[3], P. Tinyakov[19,23], I. Tkachev[19], T. Tomida[16], S. Troitsky[19], Y. Tsunesada[7,10], S. Udo[13], T. Uehama[16], F. Urban[37], D. Warren[11], T. Wong[3], M. Yamamoto[16], K. Yamazaki[28], K. Yashiro[33], F. Yoshida[21], Y. Zhezher[9,19], and Z. Zundel[3]

[1]Department of Physics, Loyola University Chicago, Chicago, IL, USA, [2]Langmuir Laboratory for Atmospheric Research, New Mexico Institute of Mining and Technology, Socorro, NM, USA, [3]High Energy Astrophysics Institute and Department of Physics and Astronomy, University of Utah, Salt Lake City, UT, USA, [4]National Institute for Space Research (INPE), Sao Jose Dos Campos, Brazil, [5]Now at NASA Marshall Space Flight Center, Huntsville, AL, USA, [6]Instituto de Recursos Naturais (IRN), Universidade Federal de Itajubá (UNIFEI) Itajubá, Minas Gerais, Brazil, [7]Graduate School of Science, Osaka Metropolitan University, Osaka, Japan, [8]Department of Physics and the Research Institute of Natural Science, Hanyang University, Seoul, Korea, [9]Institute for Cosmic Ray Research, University of Tokyo, Kashiwa, Japan, [10]Nambu Yoichiro Institute of Theoretical and Experimental Physics, Osaka Metropolitan University, Osaka, Japan, [11]Astrophysical Big Bang Laboratory, RIKEN, Wako, Japan, [12]Now at Department of Astronomy and Astrophysics, University of California, Santa Cruz, CA, USA, [13]Faculty of Engineering, Kanagawa University, Yokohama, Japan, [14]Interdisciplinary Graduate School of Medicine and Engineering, University of Yamanashi, Kofu, Japan, [15]The Graduate School of Science and Engineering, Saitama University, Saitama, Japan, [16]Academic Assembly School of Science and Technology Institute of Engineering, Shinshu University, Nagano, Japan, [17]Department of Physics, SungKyunKwan University, Suwon, Korea, [18]Department of Physics, Tokyo City University, Tokyo, Japan, [19]Institute for Nuclear Research of the Russian Academy of Sciences, Moscow, Russia, [20]Faculty of Systems Engineering and Science, Shibaura Institute of Technology, Tokyo, Japan, [21]Department of Engineering Science, Faculty of Engineering, Osaka Electro-Communication University, Osaka, Japan, [22]Now at Argonne National Laboratory, Physics Division, Lamont, IL, USA, [23]Service de Physique Théorique, Université Libre de Bruxelles, Brussels, Belgium, [24]Department of Physics, Yonsei University, Seoul, Korea, [25]Center for Astrophysics and Cosmology, University of Nova Gorica, Nova Gorica, Slovenia, [26]Faculty of Science, Kochi University, Kochi, Japan, [27]Department of Physical Sciences, Ritsumeikan University, Kusatsu, Japan, [28]College of Engineering, Chubu University, Kasugai, Japan, [29]Quantum ICT Advanced Development Center, National Institute for Information and Communications Technology, Tokyo, Japan, [30]Now at Georgia Institute of Technology, Physics Department, Atlanta, GA, USA, [31]Sternberg Astronomical Institute, Moscow M.V. Lomonosov State University, Moscow, Russia, [32]Department of Physics, School of Natural Sciences, Ulsan National Institute of Science and Technology, UNIST-gil, Ulsan, Korea, [33]Department of Physics, Tokyo University of Science, Noda, Japan, [34]Earthquake Research Institute, University of Tokyo, Tokyo, Japan, [35]Graduate School of Information Sciences, Hiroshima City University, Hiroshima, Japan, [36]Institute of Particle and Nuclear Studies, KEK, Ibaraki, Japan, [37]CEICO, Institute of Physics, Czech Academy of Sciences, Prague, Czech Republic

Key Points:

- Downward-directed TGFs were observed whose fluences bridge the gap between previous downward and satellite-detected TGFs
- The observations support the idea that satellites detect only the very strongest TGFs of a continuum
- Further multi-instrument observations are expected to provide additional insights into the causes of both short- and long-duration TGFs

Supporting Information:

Supporting Information may be found in the online version of this article.

Correspondence to:

R. U. Abbasi,
rabbasi@luc.edu

Citation:

Abbasi, R. U., Kieu, N., Krehbiel, P. R., Belz, J.W., Saba, M. M. F., Rison, W., et al. (2024). Intermediate fluence downward terrestrial gamma-ray flashes as observed by the Telescope Array Surface Detector. *Journal of Geophysical Research: Atmospheres*, *129*, e2024JD041260. https://doi.org/10.1029/2024JD041260

Received 9 APR 2024
Accepted 16 NOV 2024

Abstract On 11 September 2021, two small thunderstorms developed over the Telescope Array Surface Detector (TASD) that produced an unprecedented number of six downward terrestrial gamma ray flashes (TGFs) within one-hour timeframe. The TGFs occurred during the initial stage of negative cloud-to-ground flashes whose return strokes had increasingly large peak currents up to −223 kA, 147 GeV energy deposit in up to 25 1.2 km-spaced surface detectors, and intermittent bursts of gamma-rays with total durations up to 717 μs. The analyses are based on observations recorded by the TASD network, complemented by data from a 3D lightning mapping array, broadband VHF interferometer, fast electric field change sensor, high-speed video camera, and the National Lightning Detection Network. The TGFs of the final two flashes had gamma fluences of $\simeq 2 \times 10^{14}$ and 8×10^{14}, logarithmically bridging the gap between previous TASD and satellite-based detections. The observations further emphasize the similarity between upward and downward TGF varieties, suggesting a common mechanism for their production.

Plain Language Summary Terrestrial Gamma-Ray Flashes (TGFs) are high-energy lightning-produced radiation events that have primarily been detected by satellites, but are increasingly detected by ground-based instrumentation. While the upward satellite-detected events exhibit extremely high numbers of gamma photons, the downward ground-based versions observed by the Telescope Array Surface Detector have, until now, displayed much weaker numbers by orders of magnitude. In this paper, we report observations of downward TGFs obtained at the large-area cosmic ray detector Telescope Array facility in west-central Utah, showing strengths midway between previously detected downward TGFs and upward satellite-detected events. The results indicate that TGFs span a wide range of fluences, a finding further supported by recent airborne observations over storm tops.

1. Introduction

Terrestrial Gamma ray Flashes (TGFs) are bursts of high-energy gamma radiation that were first observed as emanating from the Earth's atmosphere by the Burst and Transient Source Experiment (BATSE) on the Compton Gamma-Ray Observatory satellite (Fishman et al., 1985, 1994). Studies soon determined that the TGFs were associated with the occurrence of lightning (e.g., Inan et al. (1996); Lehtinen et al. (1999)), but were initially thought to be caused by runaway breakdown at high altitudes (≃35 km) above the parent storms. It was not until the studies of Cummer et al. (2005) and Stanley et al. (2006) that the TGFs were indicated as being produced at lower in-cloud altitudes. Still, the issue was not fully resolved until Shao et al. (2010), utilizing improved ground-based and satellite observations of TGFs, showed not only that TGFs were produced by intracloud (IC) lightning flashes in the upper part of storms but during the first few ms of the upward negative breakdown of the flashes. The results were subsequently confirmed by Lu et al. (2010) for a RHESSI-detected TGF, utilizing a combination of observations from the North Alabama Lightning Mapping Array (LMA), Los Alamos Sferic Array (LASA), Duke University charge-moment magnetic field change observations and the National Lightning Detection Network.

Prior to the above studies, and stimulated by X- and gamma-rays being detected during balloon flights through electrified Oklahoma storms (Eack et al., 1996a, 1996b, 2000), Moore et al. (2001) reported ground-based observations of X-rays produced by negative cloud-to-ground discharges. The pioneering observations, obtained during 2000 at Langmuir Laboratory's mountain-top observatory in central New Mexico, were produced 1–2 ms immediately prior to three nearby (≃30–50 m) initial strokes to ground, whose multi-event (pileup-affected) intensities for one flash exceeded the 1.2 MeV saturation level of their NaI detector. Moore et al.'s discovery supported the idea that the downward negative stepped leaders of initial strokes to ground are capable of producing high-energy ionizing radiation ahead of advancing leader tips, providing a mechanism for the leader stepping.

In 2002 and 2004, Dwyer and colleagues at the International Center for Lightning Research and Testing (ICLRT) at Camp Blanding in Florida obtained similar X-ray observations for the dart leaders of rocket-triggered lightning flashes (Dwyer et al., 2003, 2004b). The multi-station observations confirmed the production of X-rays by dart leaders of subsequent strokes, with the 2004 observations obtained utilizing X-ray sensors with substantially improved μs temporal resolution. The observations showed that dart leader radiation was burst-like, with a spectrum of energies extending up to ≃250 keV. A subsequent study of X-ray emissions produced by stepped

leaders of initial strokes of natural lightning to ground were found to be similar to that of dart leaders (Dwyer et al., 2005).

As summarized in a recent repeat of the Langmuir X-ray experiments by Contreras-Vidal et al. (2024), the above studies initiated a nearly two decade-long sequence of observational and analytical studies of X-rays produced by rocket-triggered and natural lightning at the ICLRT and the Lightning Observatory in Gainesville (LOG). The ICLRT studies utilized increasingly sensitive, multi-station and multi-instrument observations to investigate the X-ray production by both dart and stepped negative leaders, and showed that the radiation energies extended up to ≃1–5 MeV (Howard et al., 2008; Saleh et al., 2009; Biagi & other, 2010; Hill, 2012; Schaal et al., 2012; Arabshahi et al., 2015). The studies included observations of a natural lightning flash obtained by Mallick et al. (2012) at the LOG, who reported observations of a downward negative leader during natural lightning as having photons in the MeV range, in one case possibly in excess of 5 MeV. Simultaneous X-ray measurement and high-speed video observation of the propagation of a lightning leader producing X-rays (Saba et al., 2019) found that for a dart leader, the conditions of the pre-existing channel, the amount of charge transferred by the discharge, and the orientation of the descending leader play an important role in the detection of X-rays. All together, the observations showed that energies of leader radiation extend into the transition range between X- and gamma radiation, but insufficiently so to support the relativistic runaway electron (RREA) mechanism (Dwyer et al., 2004b) as producing the radiation. Instead, the leader emissions are most likely caused by the thermal runaway mechanism, produced by strong electric fields at the tip of long conducting leaders (Celestin et al., 2015; Xu et al., 2017).

During the course of the above studies, observations were obtained of four downward gamma ray bursts, two of which happened during naturally occurring lightning (Dwyer et al., 2012; Tran et al., 2015) and two during rocket-triggered flashes (Dwyer et al., 2004a; Hare et al., 2016). The gamma bursts for the two natural flashes were produced shortly after energetic strokes to ground, while the triggered bursts were produced during strong current pulses in the initial continuing current (ICC) phase of the upward developing discharge. In both sets of cases, the bursts were more energetic than X-rays associated with negative leaders, with energies ranging up to ≃10–20 MeV.

In the present study, we report observations of six downward TGFs produced during two relatively small sequential storms on 11 September 2021 over the Telescope Array Surface Detector (TASD) network in west-central Utah. The observations follow up on previous studies at the TASD by Abbasi et al. (2018) of 10 downward TGFs observed at the TASD between 2014 and 2016 and by Belz et al. (2020) of four TGFs that occurred in 2018.

For the Abbasi et al. (2018) study, seven TGFs were compared with electrostatic field change observations of the parent lightning flashes and three were compared with 3-D VHF Lightning Mapping Array (LMA) observations of the flashes' development in space and time. In all cases, the bursts occurred during the first 1–2 ms of downward negative breakdown at the beginning of negative cloud-to-ground (−CG) flashes. The showers arrived in sequences of 2–5 short-duration (≃10 μs) bursts over time intervals of several hundred microseconds, with the initial burst or two associated with relatively strong LMA sources at an altitude of ≃3–4 km above ground level. The shower footprints on the ground were typically 2–4 km in diameter, with their cores located below the initial LMA sources. Detailed analyses of the shower footprints, associated waveforms, and the effect of atmospheric propagation showed that the showers consisted primarily of downward-beamed gamma radiation.

The result that the radiation occurred in a sequence of several short-duration bursts during the initial leader stage suggested that the TGFs were produced by energetic initial breakdown pulses (IBPs) that occur at the beginning of intra-cloud and cloud-to-ground flashes. To investigate this postulate, and to obtain high-resolution observations of the initial flash development, in 2018, we deployed our broadband VHF interferometer and fast electric field change sensor at the TASD site, 5 km east of the TASD's eastern border (Figure S1 in Supporting Information S1). From detailed observations of four TGFs obtained on two days in 2018, the TGFs were indeed shown to be correlated with strong initial breakdown pulses in the beginning few ms of flashes (Belz et al., 2020). In the process, the TGF observations showed how the initial breakdown pulses are produced, namely by recently discovered streamer-based fast negative breakdown (Tilles et al., 2019).

More recently, to better understand the optical emissions and development of lightning flashes associated with TGFs, in 2021, we installed a high-speed video camera (operating at 40,000 images per second) at the interferometer and Fast Antenna site. Shortly after installation, on September 11, a highly unusual storm system

occurred that produced an abnormally high percentage of downward TGFs—six out of the first 19 flashes over a 70 min time interval in the developing storm system. In addition to being the subject of the present study, the storm provided us with the opportunity of observing in-cloud and below cloud-base optical emissions associated with TGF production. Recently, we reported the first high-speed video camera observations of one of the TGF-producing lightning flashes (Abbasi et al., 2023), in which successive downward bursts occurred both during an initial breakdown pulse and the subsequent stepped leader stage of the ensuing cloud-to-ground stroke.

In what follows, we provide overviews of each of the six TGF-producing flashes and their TGFs. In addition to occurring quasi-successively in the storms, the final two TGFs had fluences and overall durations that were significantly more intense and longer lasting than in our previous studies at the TASD, and constitute intermediate values with the fluences and durations of satellite-detected TGFs.

2. Telescope Array (TA) and the Lightning Instruments at the TA Site

2.1. The Telescope Array Detector

The Telescope Array Surface Detector (TASD) is a 700 km^2 array comprised of 507 scintillator detectors, which provides us with the gamma ray footprints on the ground. Each TASD detector unit consists of upper and lower scintillator planes, with each plane being 3 m^2 in area and 1.2 cm thick. The upper and lower planes are separated by a 1 mm-thick steel plate, and are read out by individual photomultiplier tubes (PMTs). The output signals from the PMTs are digitized locally by a 12-bit Fast Analog-to-Digital Converter (FADC) with a 50 MHz sampling rate (Nonaka et al., 2009).

The TASD is designed to detect the charged components (primarily electrons, positrons, and muons) of the Extensive Air Showers (EAS) produced by ultra-high energy cosmic rays. The detections are recorded with 20 ns precision, with the detections at adjacent stations used to determine the parent cosmic-ray's precise direction of arrival. An event trigger occurs when three adjacent SDs observe a signal greater than 3 Minimum Ionizing Particles within 8 μs (∼ 150 FADC counts). When an event trigger occurs, the signals from all individually triggered SDs within ±32 μs are recorded (Abu-Zayyad et al., 2013).

2.2. Lightning Detectors

Observations from four types of lightning instruments were utilized in the study: A VHF Lightning Mapping Array (LMA), high-speed video camera, and a broadband VHF interferometer (INTF) and fast electric field change antenna (FA). The LMA consisted of 11 stations deployed over the 700 km^2 area of the TASD network (as shown in Figure S1 in Supporting Information S1), and locates the peak VHF radiation event in successive 80 μs time intervals in 3 spatial dimensions and time, with a timing accuracy of ≃35 *ns* rms, and over a wide (>70 dB) dynamic range, from 10 mW to more than 100 kW peak source power (Rison et al., 1999; R. Thomas et al., 2004). Cell data modems connect each station to the internet, allowing decimated data to be processed in real-time and posted on the web for monitoring purposes.

The INTF records broadband (20−80 MHz) waveforms at 180 MHz from three flat-plate receiving antennas and determines the two-dimensional azimuth and elevation arrival directions of the VHF radiation with sub-microsecond resolution (Belz et al., 2020; Stock et al., 2014), with the data being post-processed to determine the peak radiation event in successive 0.7 or 1.4 μs windows. The antennas were deployed in a triangular configuration pointed westward toward the center of the TASD, with long baselines of 121 m and a short cross-baseline of 105 m, so as to maximize the elevation angle resolution over the array. Observations from the fast electric field change antenna (FA) were recorded synchronously with INTF waveforms and provide high-resolution measurements of the low frequency (LF/ELF) discharge sferics, which are key to interpreting the INTF and LMA observations.

The monochrome Phantom V2012 operated at 40,000 frames per second (fps) with a time interval between frames of 25 μs and an exposure time of 23.84 μs (at the end of each frame the camera is blind for 1.14 μs due to data transfer). Each frame of the video is time-stamped utilizing GPS data and has a resolution of 1280 × 448 pixels. The camera is sensitive to the visible and near-infrared spectra (400–1,000 nm). It was installed inside the building housing the INTF and FA recording, allowing direct comparisons of the camera images with INTF's azimuthal versus elevation observations, as well as with the fast electric field changes being produced by the

activity being imaged. A 20-mm focal length lens provided a vertical viewing angle of 35° degrees and a horizontal angle of 84° degrees, covering almost all of the TASD stations. The camera's position and settings were optimal to observe TGF sources up to ≃30 km distance from the camera and ≃3 km above ground level. Each recorded video sequence had a duration of 1.1 s and was automatically triggered by changes in luminosity. Data from the camera were saved on a computer at the site and analyzed offline.

3. Observations and Analysis

On 11 September 2021, two storms occurred in rapid succession over the west-central to northeastern part of the TASD, between 16:00 and 18:00 UTC (10−12 a.m. local time). Figures S2 and S3 in Supporting Information S1 show LMA observations of the relatively small number of lightning flashes in the storms. The first, west-central, storm lasted ∼20 min and was marginally electrified, producing only nine flashes, but due to the low flashing rate, when lightning occurs it tends to be highly energetic. Four of the flashes in the storm were negative cloud-to-ground (−CG) discharges, with the final two flashes producing downward TGFs (The second flash of the storm went indirectly to ground, beginning with upward negative breakdown from the storm's mid-level negative charge into and then horizontally through the storm's upper positive charge as a normal polarity intracloud (IC) flash. But instead of dying out in the upper positive, the negative breakdown continued developing horizontally, exiting the storm at 8−9 km altitude northward and then turning downward as a negative leader, going to ground 82 ms later and 5−6 km horizontally distant as a 'bolt from the blue' (BFB) flash.). The other −CG flashes went directly downward to ground, with the first two having leader durations of ∼5 and 9 ms and modest return stroke currents of −39 and −26 kA, respectively. The final two TGF-producing flashes had fast, 3 ms-duration leaders and correspondingly stronger return strokes, −51 and −67 kA (flashes 8 and 9 in Figure S2 in Supporting Information S1). The strokes originated at $\sim 3.5 - 4.0$ km altitude AGL, corresponding to fast downward leader speeds of $1.2 - 1.3 \times 10^6$ m/s.

After a 35-min time period, during which two flashes occurred outside the northeastern boundary of the TASD network, lightning started up again in a new cell over the northeastern part of the TASD. Similar to the first storm, the second storm produced a relatively small number of flashes, with eight flashes occurring intermittently over a 16-min time interval (orange and red sources in Figure S2 in Supporting Information S1), prior to the storm exiting the TASD in the same northeastern location as the earlier intervening flashes. Interestingly, each of the eight flashes were −CG discharges, with four of the first six flashes producing downward TGFs. Flashes 1 and 4 of the second storm had relatively weak return stroke currents (−20 and −31 kA) and did not produce TGFs, while flashes 2, 3, 5, and 6 had increasingly strong return strokes (−53, −154, −134, and −223 kA) and produced TGFs (TGFs 3, 4, 5, and 6).

Figures 1 and 2 show observations of each of the second-storm TGF flashes, first of their VHF sources from the broadband INTF, and second of their high-speed optical images. In both instances, the panels show the sources of TGFs that occurred during successive TASD triggers, relative to the flash development. The observations are presented in the 2-dimensional elevation versus azimuth format of the INTF data, with heights above ground determined from the plan distance and elevation angle of the flashes' LMA sources. Due to the high-speed camera being located immediately adjacent to the INTF, after proper scaling and alignment the INTF sources and TGF locations could be overlaid on the optical images (Abbasi et al., 2023).

As seen in the comparisons, the TGFs of each flash (colored triangles in Figure 2) occurred either partway along or toward the end of localized downward breakdown at the beginning of the flashes, typically ≃1−2 km below the flash initiation point. Subsequent TGFs occurred at successively lower altitudes after branching began, as seen in both the INTF and optical comparisons. Flash initiation heights were typically 3−4 km above local ground level (∼1,400 m MSL) and the heights of subsequent TGFs ranged from 1.5−3.3 km above ground level. The high-speed video comparisons of Figure 2 show that the TGF events occurred both inside the cloud and as the flash began to emerge below cloud base, with subsequent triggers occurring as the branching leader developed downward to ground (blue and green triangles in Figure 2).

Figure 3 shows footprints of the TASD detections for successive triggers of the six TGFs. Whereas the footprints of TGFs 1 and 2 in the first storm are similar in size and strength as those of our previous studies (namely, 2−4 km in diameter, with energies of 10–100s of vertical equivalent muons (VEMs) (Abbasi et al., 2018; Belz et al., 2020)), the footprints in the second storm were substantially stronger than before, both in overall size and

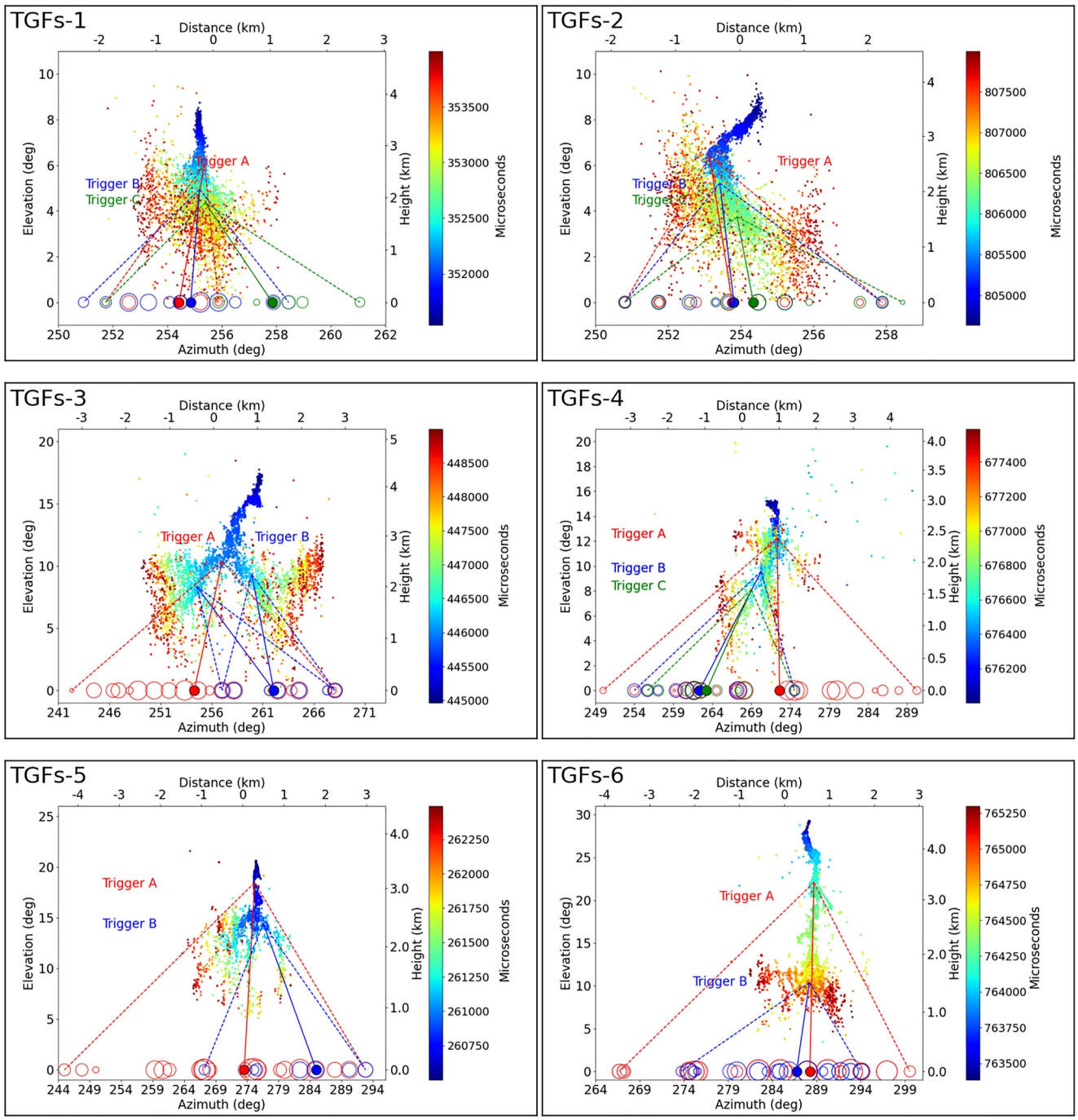

Figure 1. INTF observations of the VHF radiation sources in azimuth-elevation format for each of the TGF-producing flashes, colored by their time of occurrence and showing the locations of successive TGF trigger events. Red, green, and blue dashed lines point from the TGF source to the most distant TASD stations encompassing of the TGF's footprint, with the size of the similarly colored circles indicating the logarithmic-detected energy at each of the footprint stations. The filled circles show the energy-weighted centroid of the footprints. Note that for Trigger B of TGF 3, VHF activity was occurring simultaneously in both the left- and right-hand branches of the flash, causing there to be two possible TGF locations. Due to the right-hand branch being almost directly above the center of the TASD stations involved in its detection, the right-hand branch was most likely the source of trigger B's TGF.

total detected energy. In addition, the TGFs of first triggers were typically the strongest, particularly for the second storm. For the strongest trigger of each TGF, the gamma rays deposited spatially integrated energies of 1,541, 211, 2,049, 3,422, 21,684 and 72,110 VEM, respectively. Using the conversion factor of 2.05 MeV per VEM (where a VEM represents the energy deposited in a single TASD scintillator plane by a vertical relativistic

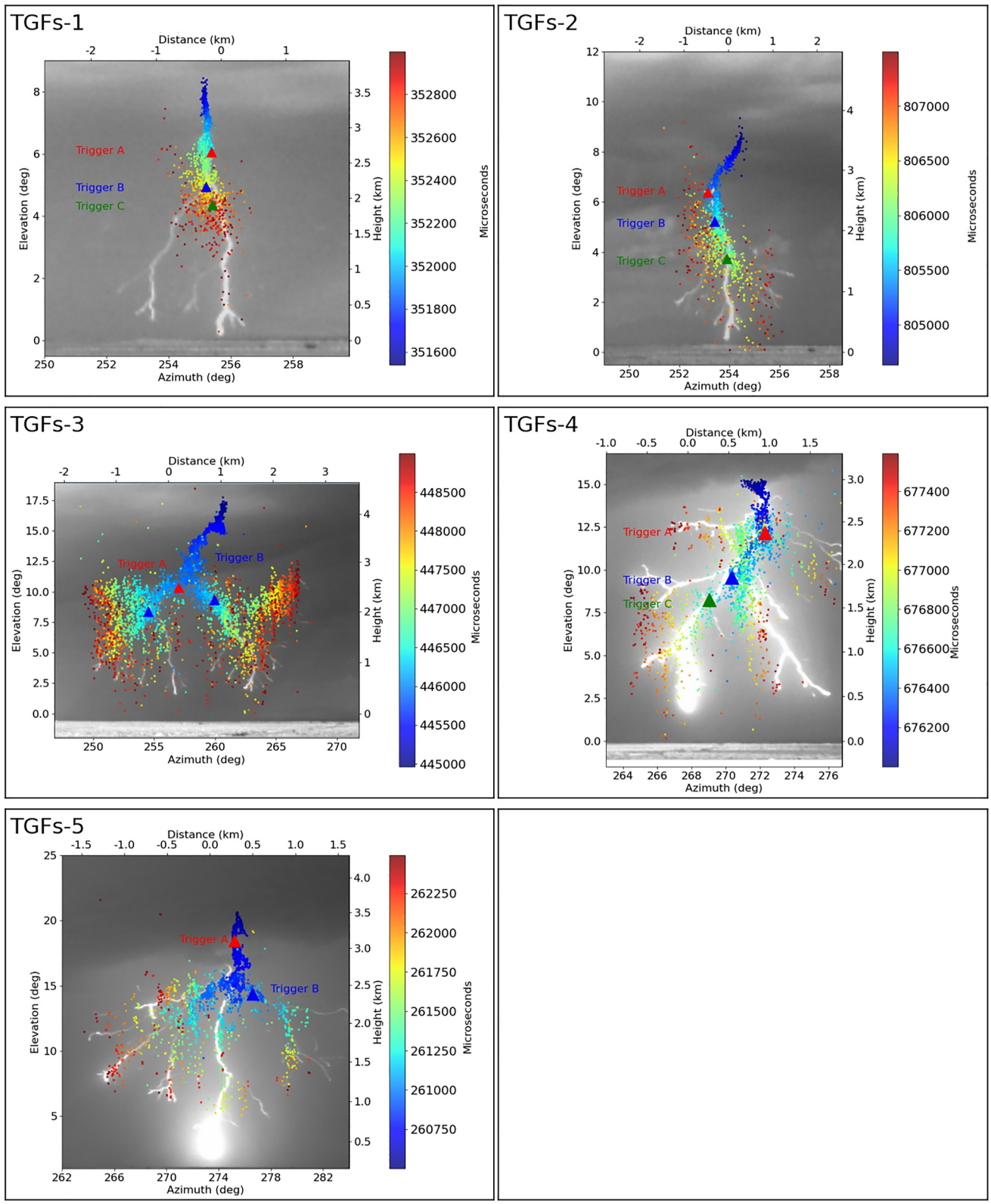

Figure 2. Comparison of INTF observations and TGF sources (filled triangles) with single-frame optical images of the flash structure below cloud base, showing the correlation of the INTF observations and TGFs with the downward leader channels. Source altitudes above ground were estimated from the LMA-detected plan distance of the overall flash.

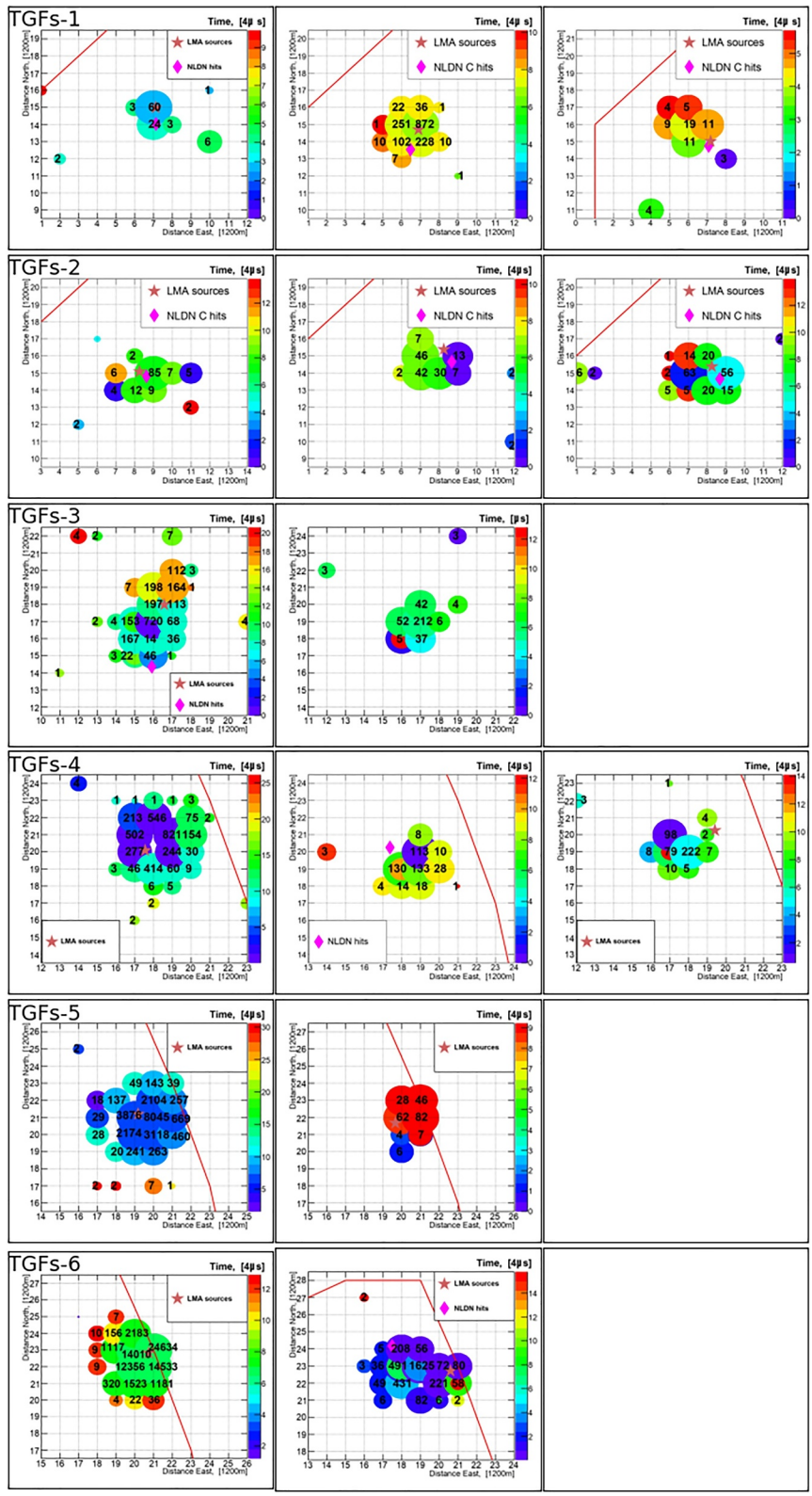

Figure 3. TASD footprints for successive TGF events of each flash, showing how the initial TGFs tend to be much stronger than subsequent TGF triggers. Circle areas are proportional to the logarithm of the energy deposit, with numbers indicating VEM deposited in each detector. Circle color indicates relative time-of-arrival in 4 μs steps. Grid spacing of the surface scintillators is 1,200 m; red lines denote the TASD border.

muon, equivalent to approximately 2.05 MeV per scintillator plane in conventional units), the deposited energies were estimated to be around 3, 0.4, 4, 7, 44, and 147 GeV, as indicated in Tables S1, S2, and S3 in Supporting Information S1.

In addition to the TASD waveforms providing information on the TGF energies, the shower footprints were analyzed using GEANT4 simulations to determine the fluences of the TGFs. As described in detail in Abbasi et al. (2018), gamma-rays above 100 keV were generated from a point-like source according to an RREA spectrum and propagated through the atmosphere to the TASD instruments. Based on the size of the shower footprint and the source altitude, the gamma ray radiation was assumed to be forward beamed within a cone half-angle of 20°. The final two TGFs, 5 and 6, had primary gamma fluences of $\simeq 2 \times 10^{14}$ and 8×10^{14}, substantially exceeding the fluences of the other TGFs in the present study as well as our previous TASD studies (Abbasi et al., 2018; Belz et al., 2020). Note that fluence calculations for TGF events typically use the RREA spectrum as a standard. However, Berge and Celestin (2019) suggest that a softer spectrum may better describe more luminous or higher fluence initial conditions for generating TGFs as observed by TA. While the TASD observations are not able to determine the spectrum of the gamma rays, investigating the possibility of softer spectra in the fluence calculations will be the subject of future work.

Figure 4 shows the complete set of the observational data for each of the six TGF flashes, providing an overview of how the TASD detections (purple vertical bars) are related to the fast electric field change observations (green traces) and the optical luminosity measurements from the high-speed camera (blue dots and traces), as discussed in Abbasi et al. (2023). The VHF sources of the downward negative leader from the beginning of the flash through the time of the first stroke to ground are shown in the background. Expanded observations encompassing the TGF occurrences are presented in the bottom panels, showing how the initial TGFs are typically associated with strong initial breakdown pulses in the beginning stages of the flashes, and to corresponding increases in the overall optical luminosities, determined in successive 25 μs intervals from successive video frames. Detailed analyses of the correlations is the subject of ongoing studies and will be reported in a future publication. The optical observations will play a new important role in the analyses, as they show strong correlations both with the overall activity and individual pulsing as the downward stepped leaders intensify.

Although the flashes of TGFs 5 and 6 were exceptionally strong, both were quenched following their return strokes. This is a characteristic feature of flashes initiated by fast leaders and high peak current return strokes, which is not fully understood. Similar quenching often leads to what are called 'lull' flashes, in which, after tens to hundreds of ms period of inactivity, the flashes reignite at the same location, producing an otherwise normal multi-stroke –CG flash (Zhang et al., 2015). However, instead of re-igniting, for about 8 ms after the −134 kA return stroke of TGF 5, the flash simply died out with a series of 10 weak (1 mW) LMA sources in the lower-altitude stepped leader region, with no further activity at altitude in or around the flash initiation region. The post-stroke activity of the stronger TGF 6 flash was even weaker, with only a single weak LMA source detected 4 ms following the −223 kA return stroke. Due to both flashes being relatively close to the INTF, their downward leaders were well-imaged by the INTF (panels 5 and 6 of Figure 1), with the LMA observations indicating relatively modest initial source powers of +26 and +34 dBW for the two flashes, respectively.

An important question to ask is why the storms produced predominantly negative cloud-to-ground flashes. This is explained by using the LMA observations to determine the charge structure of the storms (e.g., R. J. Thomas et al. (2001)). The results are presented in Supporting Figure S3 in Supporting Information S1. To begin with, the first storm had a normal tripolar charge structure in which upward intracloud (IC) flashes occurred between dominant mid-level negative and upper positive storm charges, with −CGs occurring through a somewhat weaker lower positive charge to ground (or via the upper positive charge to ground, as the bolt-from-the-blue flash). By the end of the first storm, its upper positive charge had weakened and the lower positive charge had strengthened, producing more energetic downward −CG flashes and the first two TGFs. The lack of upper positive charge and intensification of the negative and lower positive storm charges continued through the development of the second storm, with the increasing strength of the −CG flashes being indicative of low-level convective forcing pushing against an upper level cap, enhancing the mid-level negative and leaving the storm with little or no upper positive charge, that is, a dominant lower dipole of the normal tripolar structure. Although Utah storms are consistently marginally electrified, and inclined to produce energetic TGF producing storms, the particular sequence of this storm has been a rare occurrence.

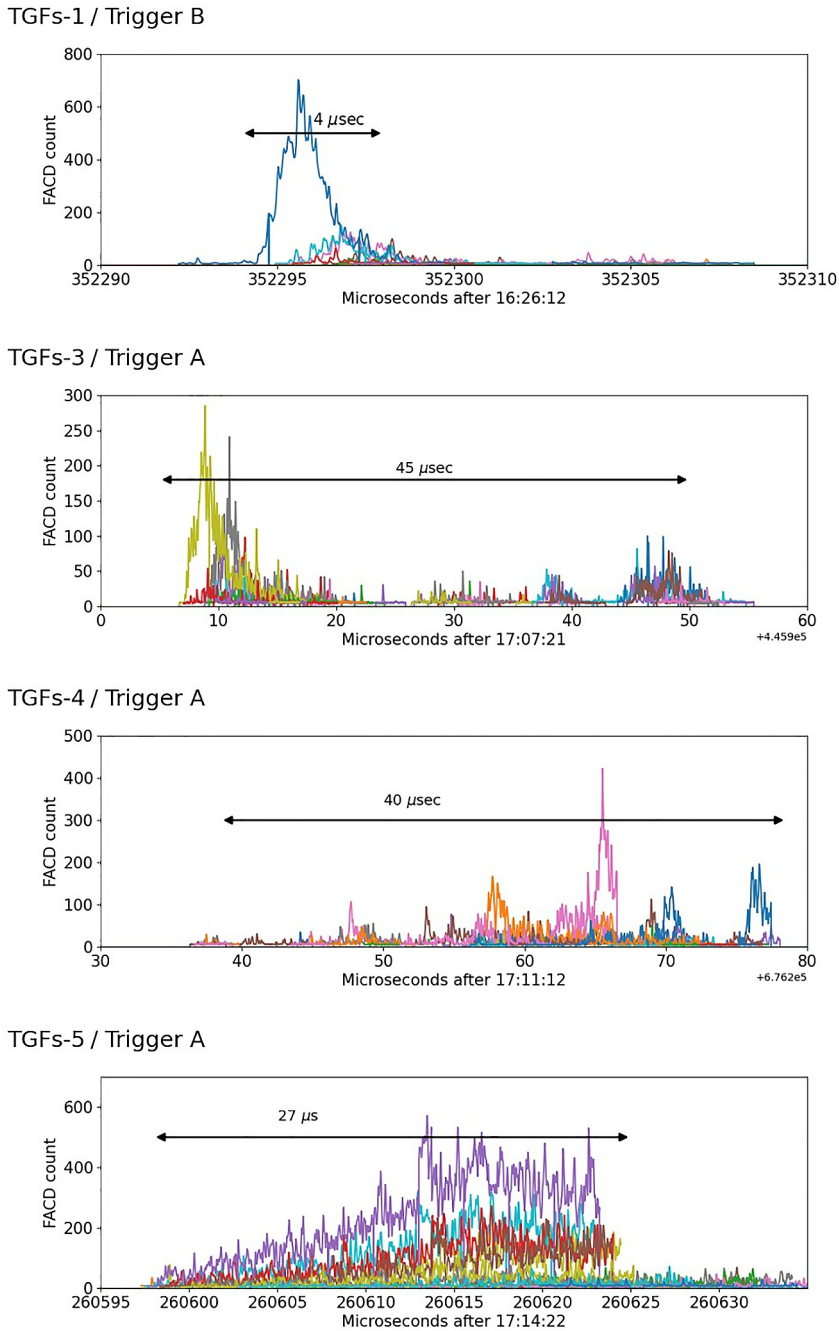

Figure 4. Observational data for each TGF from beginning of flash through time of first return stroke, and zoomed-in observations around time of TGF bursts (magenta bars), illustrating how the TGFs are associated with increases in luminosity (blue traces and horizontal arrows). Also how subsequent bursts occur later in development of downward leader, with TGFs 4 and 6 being primary examples. INTF elevation indicated by circular dots (size is proportional to the power of the radio signal); green trace shows fast E data.

Figure S4 in Supporting Information S1 compares each of the TGFs with observations of the storms obtained by the Cedar City NEXRAD weather radar. In general, the TGFs occurred within or immediately adjacent to moderately sized (~10 km diameter) reflectivity cores, with the second storm being noticeably large and stronger than the first storm. The storms were indicated as containing strong precipitation and wind shear, but weak convective available potential energy (CAPE). Additionally, the storms showed weak to average reflectivity, further indicative of weak convection.

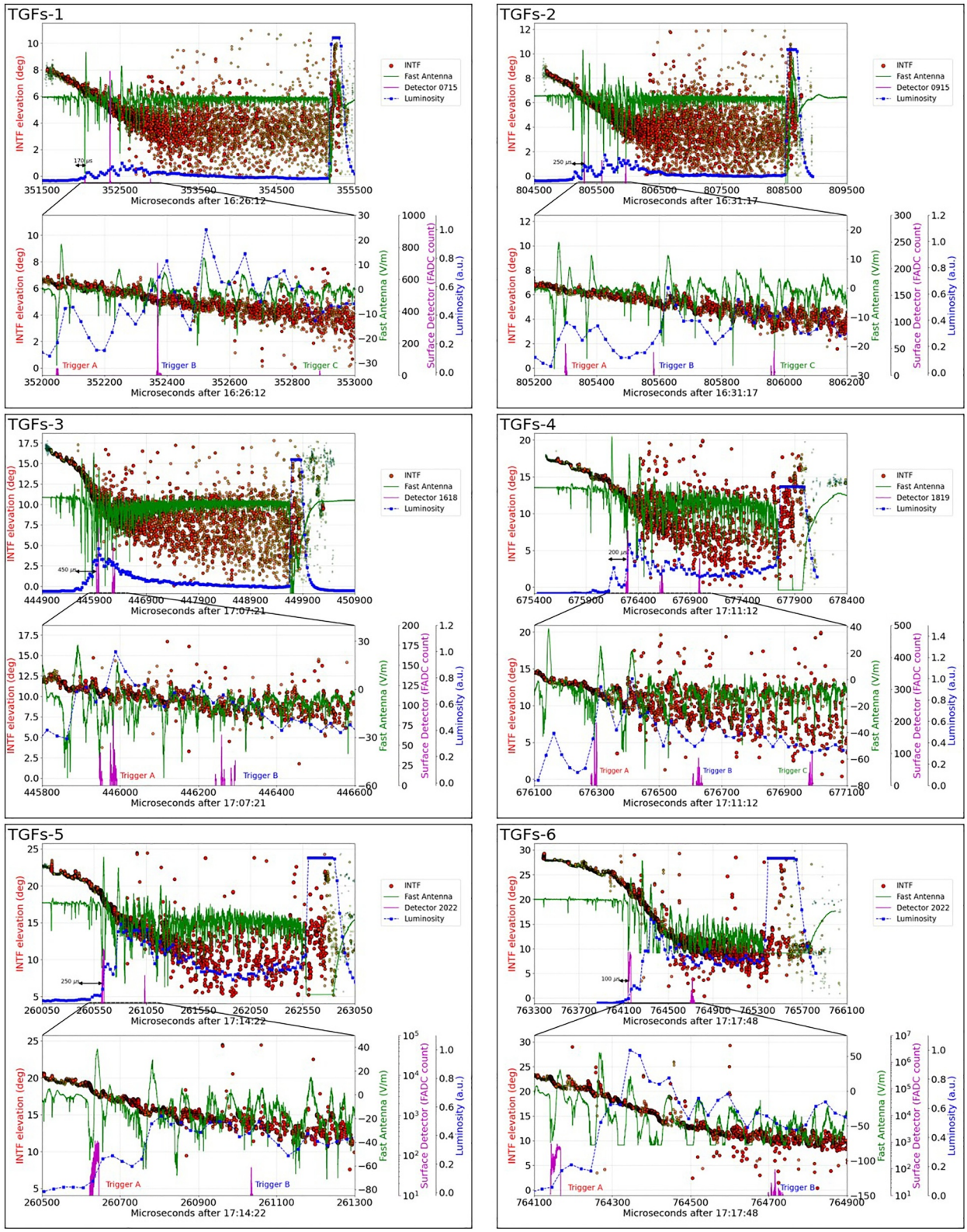

Figure 5. Example types of TASD waveforms from all participating stations. (a) Short-duration, impulsive, and localized events typical of previous observations at the TASD; (b), (c) continuously radiating examples of longer-duration events, approaching the ≃50 μs minimum durations of satellite-detected TGFs; (d) example of a high fluence (2×10^{14}) TGF, whose flux was strong enough to saturate the recording buffers at four close TASD stations, but continued significantly longer, as seen at weaker, outlying stations.

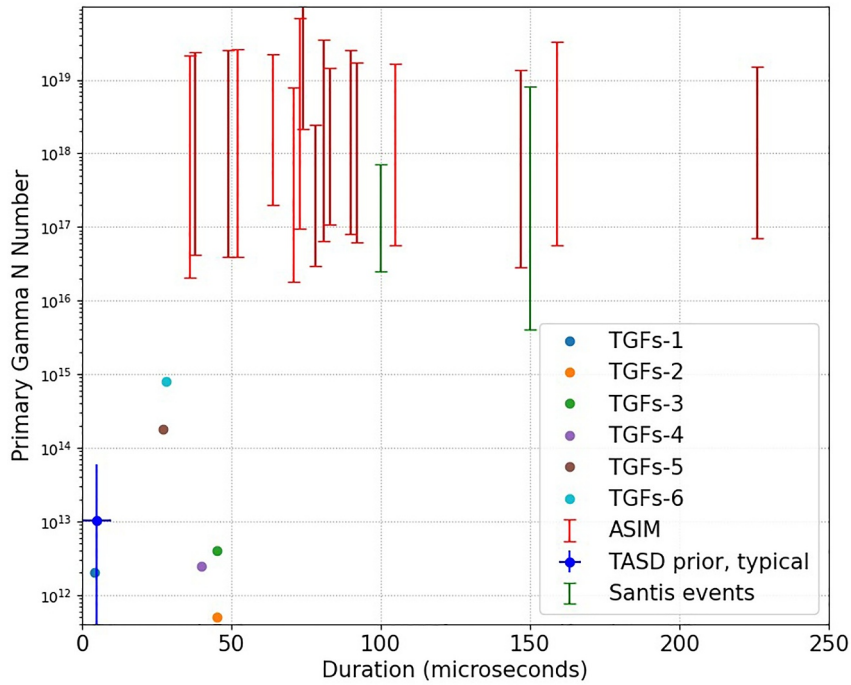

Figure 6. Comparison of fluences and durations of the present observations (colored dots) with recently summarized ASIM satellite observations (vertical red bars) (Lindanger et al., 2021) and observations of TGFs at the Säntis Tower in Switzerland (Chaffin et al., 2024), and previous TASD observations (blue dot with indicated ranges of duration and fluence values) (Abbasi et al., 2018; Belz et al., 2020), illustrating how the present observations occupy an intermediate region between the previous ground- and satellite-based TGF observations, both in fluence values and durations, suggesting that a continuum exists through the full range of fluence values and durations.

An important, final result of note from the TASD observations is that the TGFs are not always impulsive in nature, but can last for microseconds or tens of microseconds. Examples of their variability are shown in Figure 5 and Figure S5 in Supporting Information S1, whereby TGFs 3 and 4 produced somewhat intermittent but essentially continuous gamma ray radiation for 40 and 45 μsec. TGFs 5 and 6 radiated even more strongly and continuously, to the point of saturating the recording buffers after 27–28 μs, blurring the connection with individual initial breakdown pulses.

4. Summary and Discussion

The results of this study show that downward TGFs at the beginning of −CG flashes are produced not only during initial breakdown pulses (IBPs) in the first few ms of the flash, as determined by Belz et al. (2020), but also several hundred μsec later, during the stepped-leader phase of the breakdown (Abbasi et al., 2023). Another interesting result is that the initial breakdown pulse responsible for the first TGF trigger of a flash can occur below cloud base, possibly due to high cloud bases in Utah storms, making the IBPs amenable to future higher-time resolution optical photometer studies. Third, the observed TGFs are produced by flashes that have short-duration, overly fast leaders to ground, and in some cases correspondingly high peak-current return strokes. In particular, the downward leaders of TGFs 1 and 2 during the first storm both went to ground in 3 ms, and produced −51 and −67 kA return strokes. In contrast with this, two earlier −CG flashes that had leader durations of 5 and 9 ms produced weaker return strokes of −39 and −26 kA, and no TGFs. Subsequently, the flashes that produced TGFs 3, 4, 5, and 6 in the second storm had even faster leaders to ground, with durations of 4.8, 2.3, 2.4, and 2.0 ms and return stroke currents of −53, −154, −134, and −223 kA, respectively. That negative strokes to ground of TGF-producing flashes have fast downward leaders and/or high current values has been found in an increasing number and variety of studies (Dwyer et al. (2012); Tran et al. (2015); Wada et al. (2022); Ortberg et al. (2024), and Chaffin et al. (2024)).

Acknowledgments
Operation and analyses of this study have been supported by NSF grants AGS-2112709, AGS-1844306, AGS-1613260, AGS 2214044, AGS-1205727, and AGS-1720600. The support by Fundação de Amparo à Pesquisa do Estado de São Paulo —FAPESP (projects 2022/10808-4 and 2023/03908-5). The Telescope Array experiment is supported by the Japan Society for the Promotion of Science (JSPS) through Grants-in-Aid for Priority Area 431, for Specially Promoted Research JP21000002, for Scientific Research (S) JP19104006, for Specially Promoted Research JP15H05693, for Scientific Research (S) JP15H05741, for Science Research (A) JP18H03705, for Young Scientists (A) JPH26707011, and for Fostering Joint International Research (B) JP19KK0074, by the joint research program of the Institute for Cosmic Ray Research (ICRR), The University of Tokyo; by the U.S. National Science Foundation awards PHY-0601915, PHY-1404495, PHY-1404502, and PHY-1607727; by the National Research Foundation of Korea (2016R1A2B4014967, 2016R1A5A1013277, 2017K1A4A3015188, 2017R1A2A1A05071429); by the Ministry of Science and Higher Education of the Russian Federation under the contract 075-15-2024-541, IISN project No. 4.4502.13, Belgian Science Policy under IUAP VII/37 (ULB), and by National Science Centre in Poland Grant 2020/37/B/ST9/01821. The foundations of Dr. Ezekiel R. and Edna Wattis Dumke, Willard L. Eccles, and George S. and Dolores Doré Eccles all helped with generous donations. The State of Utah supported the project through its Economic Development Board and the University of Utah through the Office of the Vice President for Research. The experimental site became available through the cooperation of the Utah School and Institutional Trust Lands Administration (SITLA), U.S. Bureau of Land Management (BLM), and the U.S. Air Force. We appreciate the assistance of the State of Utah and Fillmore offices of the BLM in crafting the Plan of Development for the site. Patrick Shea assisted the collaboration with valuable advice on a variety of topics. The people and the officials of Millard County, Utah have been a source of steadfast and warm support for our work which we greatly appreciate. We are indebted to the Millard County Road Department for their efforts to maintain and clear the roads which get us to our sites. We gratefully acknowledge the contribution from the technical staffs of our home institutions. An allocation of computer time from the Center for High Performance Computing at the University of Utah is gratefully acknowledged. We thank Ryan Said and W. A. Brooks of Vaisala Inc. for providing quality NLDN

More significantly, whereas TGFs 1−4 had gamma fluences of $\simeq 2 \times 10^{12}$, 5×10^{11}, 4×10^{12} and 2.5×10^{12}, comparable to the results from our previous studies, the fluences of TGFs 5 and 6 were two to three orders of magnitude larger, namely $\simeq 2 \times 10^{14}$ and 8×10^{14}. The difference is illustrated graphically in Figure 6, which compares TASD fluences and durations with those observed by ASIM (Lindanger et al., 2021) and near the Santis Tower in Switzerland (Chaffin et al., 2024). In particular, TGFs 5 and 6 of the TASD observations are seen to be logarithmically intermediate between the less-strong events of the current and previous TASD studies, and the upward-directed ASIM satellite and Santis observations.

In addition to bridging the gap with the fluences of upward TGFs, the TASD events of the present study are found to be longer in duration than in the initial study of Abbasi et al. (2018). Examples of the range of durations have been shown in Figure 5, and are compared with ASIM and Santis observations in Figure 6. Whereas the durations extend up to 50 ms, similar to the shortest satellite detected events, the substantial difference between both the fluence and duration of satellite and downward TGFs provides a good indication that satellites are detecting only the very strongest TGFs. In addition to being supported by the present observations, it has recently been inferred by observations obtained during the 2023 ALOFT study. In this month-long NASA-funded program, and as recently reported by Bjørge-Engeland et al. (2024), overflights of a storm by NASA's high-altitude ER-2 Airborne Science Aircraft detected upward TGFs that were not detected by ASIM during a simultaneous overpass by ASIM on board the International Space Station. Coupled with numerous detections of similar upward TGFs during ALOFT, along with the present observations, implies that an entire class of TGFs exist that have intermediate fluences and durations. Just as lightning produces a continuum of X- and gamma ray emissions, the results of the present study suggest that a similar continuum exists in the fluences and durations of ground- and satellite-detected TGFs.

Data Availability Statement

The data used in this paper are available through this link: https://osf.io/ea5hr/?view. They are uploaded in the following directories: the Fast Antenna (FA), the INTerFerometer (INTF), the Lightning Mapping Array (LMA), the high-speed video camera (Optical data), and the Telescope Array Surface Detector (TASD). To be able to look at the optical data, a PCC 3.6 Phantom software is needed. The package was uploaded in the same directory.

References

Abbasi, R., Abu-Zayyad, T., Allen, M., Barcikowski, E., Belz, J. W., Bergman, D. R., et al. (2018). Gamma ray showers observed at ground level in coincidence with downward lightning leaders. *Journal of Geophysical Research: Atmospheres*, *123*(13), 6864–6879. https://doi.org/10.1029/2017jd027931

Abbasi, R., Saba, M. M. F., Belz, J. W., Krehbiel, P. R., Rison, W., Kieu, N., et al., (2023). First high-speed video camera observations of a lightning flash associated with a downward terrestrial gamma-ray flash. *Geophysical Research Letters*, *50*(14), e2023GL102958. https://doi.org/10.1029/2023GL102958

Abu-Zayyad, T., Aida, R., Allen, M., Anderson, R., Azuma, R., Barcikowski, E., et al. (2013). The surface detector array of the Telescope Array experiment. *Nuclear Instruments and Methods*, *A689*, 87–97. https://doi.org/10.1016/j.nima.2012.05.079

Arabshahi, S., Dwyer, J. R., Cramer, E. S., Grove, J. E., Gwon, C., Hill, J. D., et al., (2015). The energy spectrum of x-rays from rocket-triggered lightning. *Journal of Geophysical Research: Atmospheres*, *120*(20), 10951–10963. https://doi.org/10.1002/2015jd023217

Belz, J., Krehbiel, P. R., Remington, J., Stanley, M. A., Abbasi, R. U., LeVon, R., et al. (2020). Observations of the origin of downward terrestrial gamma-ray flashes. *Journal of Geophysical Research: Atmospheres*, *125*(23), e2019JD031940. https://doi.org/10.1029/2019jd031940

Berge, N., & Celestin, S. (2019). Constraining downward terrestrial gamma ray flashes using ground-based particle detector arrays. *Geophysical Research Letters*, *46*(14), 8424–8430. https://doi.org/10.1029/2019GL083252

Biagi, C. J., Uman, M. A., Hill, J. D., Jordan, D. M., Rakov, V. A., & Dwyer, J. (2010). Observations of stepping mechanisms in a rocket-and-wire triggered lightning flash. *Journal of Geophysical Research*, *115*(D23). https://doi.org/10.1029/2010JD014616

Bjørge-Engeland, I., Østgaard, N., Sarria, D., Marisaldi, M., Mezentsev, A., Fuglestad, A., et al. (2024). Evidence of a new population of weak terrestrial gamma-ray flashes observed from aircraft altitude. *Geophysical Research Letters*, *51*(17), e2024GL110395. https://doi.org/10.1029/2024GL110395

Celestin, S., Xu, W., & Pasko, V. P. (2015). Variability in fluence and spectrum of high-energy photon bursts produced by lightning leaders. *Journal of Geophysical Research: Space Physics*, *120*(12), 10712–10723. https://doi.org/10.1002/2015JA021410

Chaffin, J. M., Smith, D. M., Lapierre, J., Cummer, S., Ortberg, J., Sunjerga, A., et al. (2024). Mountaintop gamma ray observations of three terrestrial gamma-ray flashes at the säntis tower, switzerland with coincident radio waveforms. *Journal of Geophysical Research: Atmospheres*, *129*(2), e2023JD039761. https://doi.org/10.1029/2023JD039761

Contreras-Vidal, L., Sanchez, J. T., da Silva, C. L., Sonnenfeld, R. G., Aulich, G., Edens, H. E., et al. (2024). Spectral hardness of x- and gamma-ray emissions from lightning stepped and dart leaders. *Journal of Geophysical Research: Atmospheres*, *129*(8), e2023JD040397. https://doi.org/10.1029/2023JD040397

Cummer, S. A., Zhai, Y., Hu, W., Smith, D. M., Lopez, L. I., & Stanley, M. A. (2005). Measurements and implications of the relationship between lightning and terrestrial gamma ray flashes. *Geophysical Research Letters*, *32*(8). https://doi.org/10.1029/2005GL022778

Dwyer, J. R., Rassoul, H. K., Al-Dayeh, M., Caraway, L., Chrest, A., Wright, B., et al. (2005). X-ray bursts associated with leader steps in cloud-to-ground lightning. *Geophysical Research Letters*, *32*(1). https://doi.org/10.1029/2004GL021782

Dwyer, J. R., Rassoul, H. K., Al-Dayeh, M., Caraway, L., Wright, B., Chrest, A., et al. (2004a). A ground level gamma-ray burst observed in association with rocket-triggered lightning. *Geophysical Research Letters*, *31*(5). https://doi.org/10.1029/2003GL018771

Dwyer, J. R., Rassoul, H. K., Al-Dayeh, M., Caraway, L., Wright, B., Chrest, A., et al. (2004b). Measurements of x-ray emission from rocket-triggered lightning. *Geophysical Research Letters*, *31*(5). https://doi.org/10.1029/2003gl018770

Dwyer, J. R., Schaal, M. M., Cramer, E., Arabshahi, S., Liu, N., Rassoul, H. K., et al. (2012). Observation of a gamma-ray flash at ground level in association with a cloud-to-ground lightning return stroke. *Journal of Geophysical Research*, *117*(A10303). https://doi.org/10.1029/2012JA017810

Dwyer, J. R., Uman, M. A., Rassoul, H. K., Al-Dayeh, M., Caraway, L., Jerauld, J., et al. (2003). Energetic radiation produced during rocket-triggered lightning. *Science*, *299*(5607), 694–697. https://doi.org/10.1126/science.1078940

Eack, K. B., Beasley, W. H., Rust, W. D., Marshall, T. C., & Stolzenburg, M. (1996a). Initial results from simultaneous observation of x-rays and electric fields in a thunderstorm. *Journal of Geophysical Research*, *101*(D23), 29637–29640. https://doi.org/10.1029/96JD01705

Eack, K. B., Beasley, W. H., Rust, W. D., Marshall, T. C., & Stolzenburg, M. (1996b). X-ray pulses observed above a mesoscale convective system. *Geophysical Research Letters*, *23*(21), 2915–2918. https://doi.org/10.1029/96GL02570

Eack, K. B., Suszcynsky, D. M., Beasley, W. H., Roussel-Dupre, R., & Symbalisty, E. (2000). Gamma-ray emissions observed in a thunderstorm anvil. *Geophysical Research Letters*, *27*(2), 185–188. https://doi.org/10.1029/1999GL010849

Fishman, G. J., Bhat, P. N., Mallozzi, R., Horack, J. M., Koshut, T., Kouveliotou, C., et al. (1994). Discovery of intense gamma-ray flashes of atmospheric origin. *Science*, *264*(5163), 1313–1316. https://doi.org/10.1126/science.264.5163.1313

Fishman, G., Meegan, C., Parnell, T., Wilson, R., Paciesas, W., Mateson, J., et al. (1985). Burst and transient source experiment (BATSE) for the gamma ray observatory (GRO). In *19th international cosmic ray conference (icrc19)*.

Hare, B. M., Uman, M. A., Dwyer, J. R., Jordan, D. M., Biggerstaff, M. I., Caicedo, J. A., et al. (2016). Ground-level observation of a terrestrial gamma ray flash initiated by a triggered lightning. *Journal of Geophysical Research: Atmospheres*, *121*(11), 6511–6533. https://doi.org/10.1002/2015jd024426

Hill, J. D. a., Uman, M. A., Jordan, D. M., Dwyer, J. R., & Rassoul, H. (2012). "chaotic" dart leaders in triggered lightning: Electric fields, x-rays, and source locations. *Journal of Geophysical Research*, *117*(D3). https://doi.org/10.1029/2011JD016737

Howard, J., Uman, M. A., Dwyer, J. R., Hill, D., Biagi, C., Saleh, Z., et al. (2008). Co-location of lightning leader x-ray and electric field change sources. *Geophysical Research Letters*, *35*(13). https://doi.org/10.1029/2008GL034134

Inan, U. S., Reising, S. C., Fishman, G. J., & Horack, J. M. (1996). On the association of terrestrial gamma-ray bursts with lightning and implications for sprites. *Geophysical Research Letters*, *23*(9), 1017–1020. https://doi.org/10.1029/96GL00746

Lehtinen, N. G., Bell, T. F., & Inan, U. S. (1999). Monte Carlo simulation of runaway mev electron breakdown with application to red sprites and terrestrial gamma ray flashes. *Journal of Geophysical Research*, *104*(A11), 24699–24712. https://doi.org/10.1029/1999JA900335

Lindanger, A., Marisaldi, M., Sarria, D., Østgaard, N., Lehtinen, N., Skeie, C. A., et al., (2021). Spectral analysis of individual terrestrial gamma-ray flashes detected by asim. *Journal of Geophysical Research: Atmospheres*, *126*(23), e2021JD035347. https://doi.org/10.1029/2021JD035347

Lu, G., Blakeslee, R. J., Li, J., Smith, D. M., Shao, X., McCaul, E. W., et al. (2010). Lightning mapping observation of a terrestrial gamma ray flash. *Geophysical Research Letters*, *37*(11), L11806. https://doi.org/10.1029/2010gl043494

Mallick, S., Rakov, V. A., & Dwyer, J. R. (2012). A study of x-ray emissions from thunderstorms with emphasis on subsequent strokes in natural lightning. *Journal of Geophysical Research*, *117*(D16). https://doi.org/10.1029/2012JD017555

Moore, C. B., Eack, K. B., Aulich, G. D., & Rison, W. (2001). Energetic radiation associated with lightning stepped-leaders. *Geophysical Research Letters*, *28*(11), 2141–2144. https://doi.org/10.1029/2001gl013140

Nonaka, T., Cady, R., & Kido, E. (2009). Performance of the surface detector of the telescope array experiment. *Proceedings, 32nd International Cosmic Ray Conference (ICRC 2011): Beijing, China, August 11-18 2011*, 170.

Ortberg, J., Smith, D. M., Kamogawa, M., Dwyer, J., Bowers, G., Chaffin, J., et al. (2024). Two laterally distant tgfs from negative cloud-to-ground strokes in uchinada, Japan. *Journal of Geophysical Research: Atmospheres*, *129*(2), e2023JD039020. https://doi.org/10.1029/2023JD039020

Rison, W., Thomas, R. J., Krehbiel, P. R., Hamlin, T., & Harlin, J. (1999). A gps-based three-dimensional lightning mapping system: Initial observations in central New Mexico. *Geophysical Research Letters*, *26*(23), 3573–3576. https://doi.org/10.1029/1999gl010856

Saba, M. M. F., Ferro, M. A. S., Cuadros, E. T., Custódio, D. M., Nag, A., Schumann, C., et al. (2019). High-speed video observation of a dart leader producing x-rays. *Journal of Geophysical Research: Space Physics*, *124*(12), 10564–10570. https://doi.org/10.1029/2019JA027247

Saleh, Z., Dwyer, J., Howard, J., Uman, M., Bakhtiari, M., Concha, D., et al. (2009). Properties of the x-ray emission from rocket-triggered lightning as measured by the thunderstorm energetic radiation array (tera). *Journal of Geophysical Research*, *114*(D17). https://doi.org/10.1029/2008JD011618

Schaal, M. M., Dwyer, J. R., Saleh, Z. H., Rassoul, H. K., Hill, J. D., Jordan, D. M., & Uman, M. A. (2012). Spatial and energy distributions of x-ray emissions from leaders in natural and rocket triggered lightning. *Journal of Geophysical Research*, *117*(D15). https://doi.org/10.1029/2012JD017897

Shao, X., Hamlin, T., & Smith, D. M. (2010). A closer examination of terrestrial gamma ray flash related lightning processes. *Journal of Geophysical Research*, *115*(A6), A00E30. https://doi.org/10.1029/2009ja014835

Stanley, M., Shao, X., Smith, D. M., Lopez, L. I., Pongratz, M. B., Harlin, J. D., et al. (2006). A link between terrestrial gamma-ray flashes and intracloud lightning discharges. *Geophysical Research Letters*, *33*(6), L06803. https://doi.org/10.1029/2005gl025537

Stock, M. G., Akita, M., Krehbiel, P. R., Rison, W., Edens, H. E., Kawasaki, Z., & Stanley, M. A. (2014). Continuous broadband digital interferometry of lightning using a generalized cross-correlation algorithm. *Journal of Geophysical Research: Atmospheres*, *119*(6), 3134–3165. https://doi.org/10.1002/2013jd020217

Thomas, R., Krehbiel, P. R., Rison, W., Hunyady, S. J., Winn, W. P., Hamlin, T., & Harlin, J. (2004). Accuracy of the lightning mapping array. *Journal of Geophysical Research*, *109*(D14), D14207. https://doi.org/10.1029/2004jd004549

Thomas, R. J., Krehbiel, P. R., Rison, W., Hamlin, T., Harlin, J., & Shown, D. (2001). Observations of vhf source powers radiated by lightning. *Geophysical Research Letters*, *28*(1), 143–146. https://doi.org/10.1029/2000GL011464

Tilles, J., Liu, N., Stanley, M. A., Krehbiel, P. R., Rison, W., Stock, M. G., et al., (2019). Fast negative breakdown in thunderstorms. *Nature Communications*, *10*(1648), 11776–11786. https://doi.org/10.1038/s41467-019-09621-z

Tran, M., Rakov, V., Mallick, S., Dwyer, J., Nag, A., & Heckman, S. (2015). A terrestrial gamma-ray flash recorded at the lightning observatory in gainesville, Florida. *Journal of Atmospheric and Solar-Terrestrial Physics*, *136*, 86–93. (Advances in Lightning Research). https://doi.org/10.1016/j.jastp.2015.10.010

Wada, Y., Morimoto, T., Nakamura, Y., Wu, T., Enoto, T., Nakazawa, K., et al. (2022). Characteristics of low-frequency pulses associated with downward terrestrial gamma-ray flashes. *Geophysical Research Letters*, *49*(5), e2021GL097348. https://doi.org/10.1029/2021GL097348

Xu, W., Marshall, R. A., Celestin, S., & Pasko, V. P. (2017). Modeling of x-ray images and energy spectra produced by stepping lightning leaders. *Journal of Geophysical Research: Atmospheres*, *122*(21), 11776–11786. https://doi.org/10.1002/2016JD026410

Zhang, Y., Krehbiel, P. R., Edens, H. E., & Stock, M. (2015). Observations of high peak current 'lull' lightning flashes. In *Agu fall meeting abstracts* (Vol. 2015, p. AE13A-07).